Food Packaging and Shelf Life 42 (2024) 101263

Contents lists available at ScienceDirect

Food Packaging and Shelf Life

journal homepage: www.elsevier.com/locate/fpsl

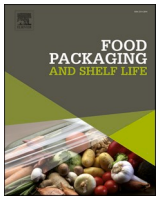

Detecting ultraviolet C radiation under polyethylene terephthalate (PET) packaging by thermoluminescence analysis using commercial dosimeters

C. Boronat [a,b,*], V. Correcher [b], J.C. Bravo-Yagüe [c]

[a] Department of Inorganic Chemistry, Faculty of Sciences, National University of Distance Education (UNED), Av. de Esparta s/n, 28232 Madrid, Spain
[b] Department of Environment, Centre for Energy, Environment and Technology Research (CIEMAT), Av. Complutense 40, 28040 Madrid, Spain
[c] Department of Analytical Sciences, Faculty of Sciences, National University of Distance Education (UNED), Av. de Esparta s/n, 28232 Madrid, Spain

ARTICLE INFO

Keywords:
Polyethylene terephthalate
Food packaging
Ultraviolet C radiation
Fourier transform infrared spectroscopy
Thermoluminescence

ABSTRACT

Food irradiation is a proven technology that enhances food quality and safety by removing microorganisms and extending shelf life. Ultraviolet C radiation (UVC) has recently attracted interest due to its potential to inactivate foodborne pathogens. It relies on several advantages; however, there is limited research on its efficacy and safety particularly concerning food packaging materials such as polyethylene terephthalate (PET).

This study reports on the effect of UVC radiation on commercial thermoluminescence dosimeters (namely, TLD-100, TLD-200, TLD-400 and GR-200) placed under PET films with different thicknesses (0.10, 0.42, and 0.60 mm). The results indicate the potential use of these materials for the detection of UVC radiation passing through the randomly selected PET samples. Fourier transform infrared spectroscopy assesses potential structural and chemical alterations in the PET induced by UVC exposure.

1. Introduction

Food irradiation is a technology that has been employed for many years to enhance the quality and safety of food products. The Food and Drug Administration (FDA) has approved several food irradiation methods, including gamma rays (with ^{60}Co or ^{137}Cs radioisotopes), electron beams (with high energy reaching up to 10 MeV), X-rays (with high energy reaching up to 5 MeV) and, most recently, ultraviolet (UV) radiation (at a wavelength of 253.7 nm) (Ghazala, 2020). These methods are effective in eliminating and/or reducing harmful bacteria and parasites in food products, as well as in extending their shelf life (Ben--Fadhel et al., 2021; Prajapati, Asrey, Varghese, Singh, & Pal Singh, 2021; Soro et al., 2021; Tao et al., 2019). Specifically, UVC exposure (in the range of 200–280 nm) can be a useful tool to inactivate pathogenic bacteria in food and food contact surfaces (Belović, Kevrešan, Pestorić, & Mastilović, 2015; Prajapati et al., 2021). This technology offers several advantages to ensure food safety, such as: (i) germinal ability to damage the DNA of pathogenic microorganisms, (ii) does not produce chemical residues, (iii) color, texture, flavor and even enzyme activity are preserved, (iv) it is a simple, cold and dry process, (v) requires low maintenance and (vi) is an inexpensive method (Guerrero-Beltrán & Barbosa-Cánovas, 2004). However, the use of UVC irradiation in food processing is still an emerging technology, and there is limited research on its efficacy and safety compared to those material which are designed to pharmaceutical products or medical devices (Foschi, Giorgi, Ambretti, Lazzarotto, & Violante, 2023).

Prior to irradiation, food is typically packaged (Ghazala, 2020), and implementing this methodology requires addressing at least two essential aspects: (i) determine the potential damage that the radiation exposure could induce in the polymer (polyethylene terephthalate -PET- in this case) usually employed as commercial packaging material, and (ii) detect the UVC irradiation. For such purposes, there are two optimal techniques that allow determining both items, namely, Fourier transform infrared spectroscopy (FTIR) and thermoluminescence (TL). Despite the significance of these techniques, there has been a scarcity of studies involving them in the analysis of food packaging materials exposed to UVC radiation, particularly polymeric materials like PET (Chun, Kim, Lee, Yu, & Song, 2010; Jamalzadeh & Sobkowicz, 2022). PET, which is widely used in food packaging applications, stands out as a highly favorable material due to its stability, cost effectiveness, light weight nature, flexibility, transparency, acceptable recyclability and its excellent barrier, among others (Fernández-Menéndez, García-López, Argüelles, Fernández, & Viña, 2020; Zhang et al., 2022).

UVC radiation could induce alterations in the chemical and physical

* Corresponding author at: Department of Inorganic Chemistry, Faculty of Sciences, National University of Distance Education (UNED), Av. de Esparta s/n, 28232 Madrid, Spain.
E-mail addresses: cecilia.boronat@ccia.uned.es (C. Boronat), v.correcher@ciemat.es (V. Correcher), juancarlos.bravo@ccia.uned.es (J.C. Bravo-Yagüe).

https://doi.org/10.1016/j.fpsl.2024.101263
Received 27 November 2023; Received in revised form 6 February 2024; Accepted 24 February 2024
Available online 7 March 2024
2214-2894/© 2024 The Author(s). Published by Elsevier Ltd. This is an open access article under the CC BY-NC-ND license (http://creativecommons.org/licenses/by-nc-nd/4.0/).

properties of the polymers (Andrady et al., 2023) including: (i) *photo--oxidation*, breaking chemical bonds in the polymer, leading to chain fragmentation and a subsequent reduction in mechanical strength; (ii) *radical formation*, initiating additional polymerization or degradation reactions; (iii) *bleaching effect*, disrupting pigments or colorants present in PET; (iv) *reduced fatigue resistance*, making it more susceptible to cracking or failure under cyclic loads; (v) *introduction of functional groups*, into the polymer structure, altering its chemical and physical properties; and/or, (vi) *changes in optical properties*, affecting characteristics such as transmittance and reflectance (Andrady et al., 2023). In this sense, FTIR provides a method for analyzing such potential conformational changes and microscopic deformations in food packaging plastic films. FTIR, which is a vibrational spectroscopy technique based on the fundamental vibrational motions of functional groups within the polymeric lattice, provides structural insights at the molecular level without the need for chemical or physical pre-treatment of samples (Hu, Huyan, Ding, Dong, & Yu, 2020; Junqueira-Gonçalves, Alarcón, & Niranjan, 2013; Paiva, Wrona, Nerín, & Cruz, 2022).

On the other hand, while food irradiation is approved in almost 60 countries (Ghazala, 2020), there is currently no established method to discriminate UV-irradiated food, which would allow regulatory authorities to rely on a tool to certify correct labeling or validate a standard procedure to determine the total absorbed dose, among others similar to the EN 1788 standard procedure (EN, 1788, 2001). This tool would be based on identifying irradiated food through changes in biological, chemical, and physical properties (Correcher & Garcia-Guinea, 2011, 2013). In this context, TL technique appears as one of the most suitable, effective, cost efficient and accurate method for such purpose. TL relies on the emission of light from a dielectric solid sample (insulator or semiconductor) when it is heated after being irradiated (artificially or naturally) by ionizing or partially ionizing radiation. During the analytical heating, a photomultiplier tube detects the TL signal, which is recorded as a function of wavelength or temperature. The resulting curve, known as a glow curve or TL curve, exhibits luminescent intensity and shape patterns that correspond to radiation dose and heating rate (McKeever, 1986).

There are several detectors and dosimeters that have the capability of detecting and recording UVC radiation, including electronic devices and synthetic dosimeters with different compositions, i.e., TLD-100 (LiF: Ti, Mg), TLD-200 (CaF_2: Mn), TLD-400 (CaF_2: Dy) and GR-200 (LiF: Mg, Cu, P), among others (Boronat et al., 2023). As a result, TL analysis, among other techniques, is essential for determining the structures, compositions, typomorphic properties and genetic characteristics of materials. In this context, intrinsic, structural, surface and extrinsic defects contribute to distinct luminescence emissions.

This study reports on the preliminary findings regarding the effect of UVC radiation on commercial dosimeters (namely, TLD-100, TLD-200, TLD-400 and GR-200) placed under PET films with different thicknesses (0.10, 0.42 and 0.60 mm) to determine their UVC-TL responses exposed to radiation through the plastic. Additionally, PET samples have been characterized by FTIR spectroscopy to analyze potential changes in the plastic structure due to UVC exposure.

2. Materials and methods

This study was performed on PET samples with different thickness of 0.10 mm (PET 1), 0.42 mm (PET 2) and 0.60 mm (PET 3), randomly selected from grocery stores at Madrid (Spain).

The structural characterization of the plastic materials was carried out by means of ATR-FTIR spectroscopy. Infrared absorption spectra of the samples were measured at room temperature (RT) within the wavenumber range from 4000 to 400 cm^{-1}, employing a Spectrum FT-IR-4100 spectrometer equipped with the ATR PRO ONE Accessory (ATR-FTIR) and using Spectra Manager® software, provided by JASCO (Tokyo, Japan). The spectral resolution employed for the measurements was 4 cm^{-1}.

UVC exposure consisted of 1 h at RT was performed on an automated irradiator developed at CIEMAT (Delgado, Unamuno, Muñiz, Correcher, & Gómez Ros, 1996). It allows UV illumination with a TUV-6 W Hg lamp (254.7 nm, 0.03 $W{\cdot}m^2$ of UV irradiance value at 10 cm). Commercial dosimeters, namely LiF: Ti, Mg (TLD-100), CaF_2: Dy (TLD-200), CaF_2: Mn (TLD-400), provided by Harshaw Chemical Company (Ohio, USA) with sizes of 0.32 × 0.32 × 0.09 cm^3 each one, and LiF: Mg, Cu, P (GR-200) disks of 4.5 Ø 0.8 mm^3 dimensions supplied by Beijing Shiying Radiation Detector Works (China), were used as UVC detectors. These dosimeters were placed under the PET samples to investigate the extent of radiation that can penetrate through the plastic and potentially reach the food during post-packaging irradiation.

Before the subsequent irradiation, dosimeters were formerly annealed at 400 ± 1 °C for 1 h employing the electrical oven to eliminate any residual data and 1 h of cooling rate. The effect of UVC radiation was assessed by examining the TL properties of the mentioned detectors. TL measurements were performed employing an automated Risø TL reader model TL DA-12 provided with an EMI 9635 QA photomultiplier (Bøtter-Jensen & Duller, 1992). The emission was studied through a FIB002-blue filter (provided by Melles-Griot Company) peaked at 320 - 480 nm, 80 ± 16 nm of FWHM and 60% of transmittance. The TL reader is also supplied with a ^{90}Sr / ^{90}Y source with a dose rate of 0.011 $Gy{\cdot}s^{-1}$ calibrated with a ^{137}Cs photon source in a secondary standard laboratory (Correcher & Delgado, 1998). All the TL measurements were obtained using a linear heating rate of 5 $°C{\cdot}s^{-1}$ from room temperature up to 400 °C in a N_2 atmosphere. A second TL readout of the TLDs to obtain the background due to the incandescence and detector noise; it was directly subtracted from the TL data.

3. Results and discussion

3.1. Sample characterization: FTIR spectroscopy

FTIR spectroscopy has been employed to investigate potential variations in the structural and chemical properties of PET samples, which is a material commonly used in food packaging applications (Fernández-Menéndez et al., 2020; Zhang et al., 2022). The aim of this characterization is to comprehensively assess the influence of UVC radiation on PET samples with different thicknesses, a factor that could significantly affect the ability of UVC to irradiate the packaged food. PET is a well-known thermoplastic polymer synthesized through the polymerization of repetitive ethylene terephthalate units, as illustrated by the following chemical formula in Fig. 1A.

According to Day & Wiles (1972), UV exposure could induce an increase in the concentration of carboxylic acid end groups (–COOH) and the generation of volatile products (CO and CO_2) and free radicals. This phenomenon is commonly referred to as the *photo-oxidation* process, shown in Fig. 1B.

These authors explained the distinction between the *photolysis process*, which occurs under vacuum conditions, and *photo-oxidation process*, which takes place in the presence of oxygen (an aspect directly relevant to our current investigation). Consequently, no disparities in the composition of the volatile products were observed when the experiments were performed in ambient air instead of vacuum conditions. However, there was a notable increase in the production of CO_2. This discrepancy suggests the participation of oxygen in the reactions responsible for CO_2 formation in the presence of air. Furthermore, the quantum yields for the initial rates of CO and –COOH end groups formation was nearly identical to those achieved under vacuum conditions. This consistency can be explained with the same primary reactions, specifically reaction [2] (Fig. 1B) following a primary photolytic chain scission sequence to yield CO, and reaction [3] (Fig. 1B) via a *Norrish* type II photoelimination mechanism to generate –COOH. Additionally, the enhanced production of CO_2 under UV irradiation in the presence of air can likely be attributed to the formation of hydroperoxides (reactions [4–8], Fig. 1B).

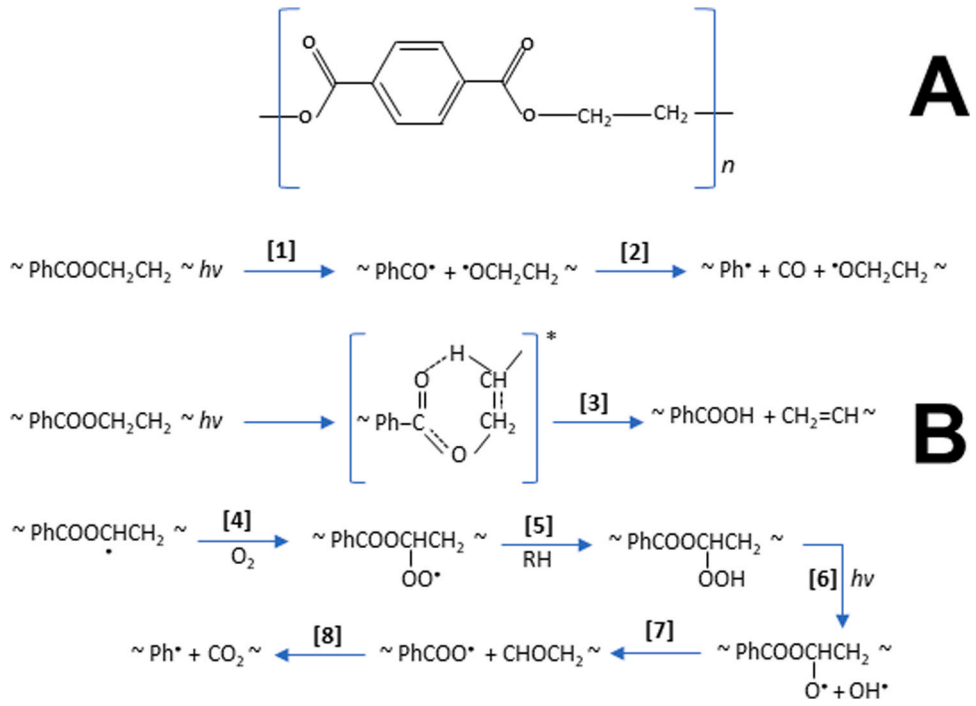

Fig. 1. (A) Molecular structure of polyethylene terephthalate ($PhCOOCH_2CH_2$), composed of terephthalate (C_6H_4COO) units intricately linked to ethylene ($–CH_2–CH_2–$) moieties. And (B) Photo-oxidation process of PET due to UVC radiation. (adapted from Day & Wiles, 1972).

FTIR spectroscopy enables us to gain insights into the formation of free radicals and volatile products, and subsequently confirm their potential presence through spectral analysis. For such purpose, Fig. 2 (A-C) displays FTIR spectra (from 4000 to 400 cm^{-1}) comparing non-irradiated and 1-hour UVC-irradiated PET samples with different thicknesses. Additionally, to enhance clarity, the response has been normalized and is presented in Fig. 2 (D-F), which reveals possible differences in the signal following UVC irradiation. Furthermore, the assignment of the observed FTIR bands is provided in Table 1. The conventional procedure of plotting transmission (in %) against wavenumber (in cm^{-1}) has been adhered to, where the identified minima in the transmission spectra correspond to the absorption peaks associated with the molecules and functional groups.

As appreciated in Fig. 2 (A-C), both non-irradiated and 1-hour UVC-irradiated PET samples exhibit characteristic bands corresponding to the vibrational modes of the polyethylene terephthalate molecule (as depicted in Fig. 1 A). These distinctive FTIR peaks, prominently delineated in Fig. 2 (A-C), are present in the current infrared absorption spectrum and offer insights into the strength of the bonds within the material, as explained below. The FTIR spectra suggest that the extent of damage to various polymer bonds is negligible. However, it is important to note that other studies have demonstrated that such alterations in bond strength increase with longer irradiation times (Fechine, Souto-Maior, & Rabello, 2007; Giaganini et al., 2023; Mikac et al., 2023).

The vibrational modes of C–H stretching is characterized by their strength, and they appear at higher wavenumbers within different aromatic and aliphatic groups. These functional groups, which include alkyl ($–CH_3$, $–CH_2$, and –CH), alkanal (–CHO), alkyn (–C≡C–), alken (–C═C–), and arene (aromatic hydrocarbons), are discernible as absorption peaks in the range of 3300–2840 cm^{-1}. Conversely, the vibrational mode of C–H bending exhibits weaker bond strength when compared to their stretching counterparts. These bending modes are prevalent within the alkyl and alkene groups, appearing as absorption peaks in the ranges of 1465–1375 cm^{-1} and 995–885 cm^{-1}, respectively. In the case of arene, both in-plane and out-of-plane C–H bending modes are evident within the regions of 1300–1000 cm^{-1} and 900–650 cm^{-1}, respectively (Donelli, Freddi, Nierstrasz, & Taddei, 2010; Prasad, De, & De, 2011).

In the context of the O–H stretching mode, it is observed in alkanol (C_nH_{2n+2}–OH) and carboxylic acid end group (–COOH) within the infrared absorption spectra, specifically within the range of 3550–2500 cm^{-1}. The vibrational mode of C═O stretching occurs in various compounds, including aliphatic ketones, alkanals, aromatic ketones, alkanoic acids, alkanoyl chlorides and alkanoate esters, presenting itself in the spectral region of 1815–1680 cm^{-1}. In the carbonyl group, characteristic infrared spectra in the range of 1720–1706 cm^{-1} correspond to C═O stretching. Furthermore, the C═O stretching modes inherent to alkanoate esters and alkoxy ethers are characterized by distinct peaks within the spectral bounds of 1310–1020 cm^{-1} (Donelli et al., 2010; Prasad et al., 2011).

Specific molecular groups, such as ethylene glycol, para-substituted phenyl ring or the *trans*-configuration $\delta(CH_2)$, as well as the C═C stretch within the phenyl ring and the H vibrations attached to the phenyl ring δ(CH), can be identified at spectral positions of 1505, 1453, 1242, and 1016 cm^{-1}, respectively. In ethylene glycol, the *trans*-configuration-ν(CO) and -$\nu(CH_2)$ exhibit signature absorption peaks in the range of 980–850 cm^{-1}. Additionally, the absorption peak at 873 cm^{-1} is attributed to H vibrations attached to the phenyl ring-ν(CH) (Donelli et al., 2010; Prasad et al., 2011).

Many of the remaining bands exhibit variations based on the processing history of the material, whether it has undergone extrusion and quenching or heat treatment and drawing processes. These processing steps result in distinct *amorphous* or *crystalline* states, respectively. These variations can be attributed to alterations in the configuration of the phenylene carbonyl bonds and ethylene glycol group, involving *cis/trans* conformers. The IR spectra display split absorption bands, indicating differences in the force field within the *amorphous* and *crystalline* regions, as well as differences in the chain conformation surrounding glycol ester groups (Chen, Hay, & Jenkins, 2012).

In *crystalline* regions, the *trans* isomer predominates while in *amorphous* regions, a dynamic equilibrium between *cis* and *trans* conformers

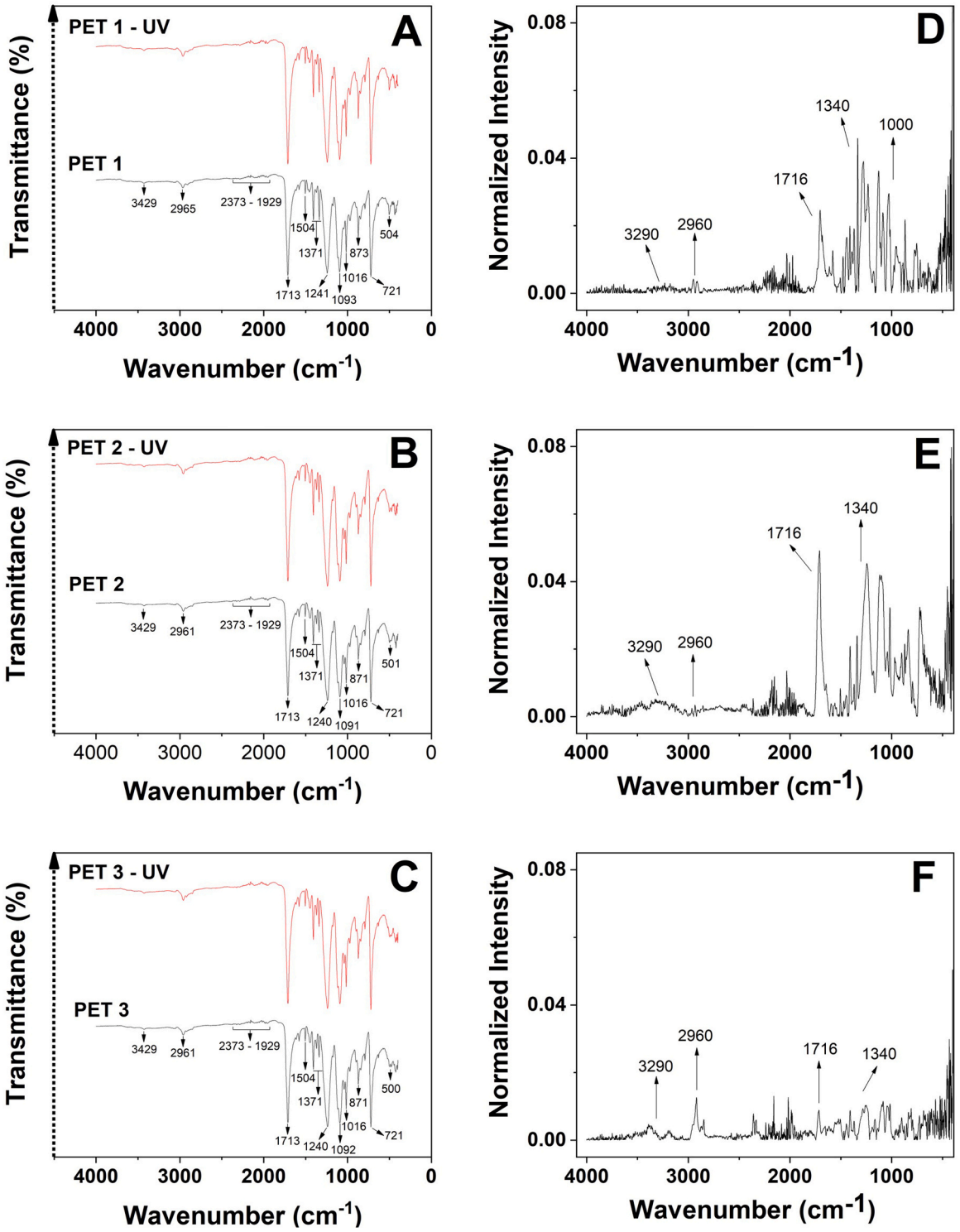

Fig. 2. FTIR and Normalized FTIR spectra of non-irradiated and UVC irradiated PET food packaging samples with different thicknesses: (A and D) PET 1 (0.10 mm), (B and E) PET 2 (0.42 mm) and (C and F) PET 3 (0.60 mm). Note that the signal of the UVC-irradiated PET samples has been intentionally shifted to avoid spectral overlap.

is observed. Factors such as temperature or other forms of energy (i.e., UVC radiation), can induce a transition from the *gauche* to the *trans* form, resulting in an increase in *crystalline* content. Such crystallization can also be influenced by stretching, depending on the temperature, which has led to debates regarding the precise assignments of absorption bands in the IR spectrum concerning crystallinity and changes in chain conformation (Table 1). Specifically, the bands at 1471, 1341, 1123, 972, and 849 cm^{-1} serve as markers for the *crystalline* structure of PET in its *trans* configuration, whereas bands at 1371, 1044, and 898 cm^{-1} characterize the *amorphous* form with a *cis* configuration (Donelli et al., 2010). Conformational changes in the material are associated with variations in optical density and alterations in polymer density and electrical properties, particularly within the structured (*trans*) regions. These alterations lead to a decrease in polarization and dielectric constant, and the extent of variations in the loss tangent and dielectric strength depends on the reduction in molecular mass (Chen et al., 2012).

Table 1
Assignment of vibrational modes for observed FTIR bands in PET food packaging samples.

Wavenumber (cm^{-1})						Assignation	Conformation
PET1	PET1 - UVC	PET2	PET2 - UVC	PET3	PET3 - UVC		
3424	3424	3424	3427	3428	3429	O-H stretching (Hydroxyl groups)	*Crystalline*
3290	3290	3290	3290	3293	3293	O-H stretching (Carboxylic acid end groups)	–
2964	2964	2960	2960	2960	2958	C-H stretching (Aromatic and aliphatic)	*Amorphous, cis*
–	2164	–	2164	–	2166	CO stretching vibration	–
2107	2106	2111	2114	2108	2107	C-H stretching (Aromatic skeleton)	–
1710	1710	1712	1712	1711	1712	C═O stretching (Carboxylic acid end groups)	*Crystalline*
1575	1579	1578	1578	1578	1578	C═C stretching (Aromatic skeleton)	*Amorphous*
1505	1503	1504	1505	1505	1505	Para-substituted benzene ring, C═C stretching (Aromatic skeleton) and CH in-plane bending ring	*Crystalline*
1453	1453	1447	1447	1446	1449	CH_2 bending and O-CH bending	*Amorphous, cis/ gauche*
1406	1406	1408	1408	1407	1408	Para-substituted benzene ring, CH in-plane bending (Aromatic skeleton) and CC stretching	–
1339	1339	1341	1341	1341	1341	OCH bending, C–C Alkane, $=CH_2$ wagging, bending and wagging vibrational modes of the ethylene glycol	*Crystalline, trans*
1242	1242	1238	1238	1239	1240	C═C stretching (phenyl ring), C(=O)-O stretching and C═O in-plane bending	*Amorphous, cis*
1172	1172	1175	1175	1176	1175	Aromatic – 1, 4 substituted ring and ring CH in-plane bending	–
1093	1095	1091	1092	1091	1090	Methylene group and C-O stretching (ester group)	–
1016	1016	1016	1016	1016	1016	C–H in-plane stretching, ring CCC bending and ring CH in-plane bending	*Amorphous, gauche*
872	872	870	871	871	871	Para-substituted benzene ring, ring CH out-of-plane bending, ring-ester C-C out-of-plane bending, C═O out-of-plane bending and ring torsion	–
790	790	792	792	792	792	ring CH out-of-plane bending, C═O rocking and CCO bending	–
722	722	722	722	722	722	C═O out-of-plane bending, ring torsion and ring C═H out-of-plane bending	*Crystalline*
502	501	497	499	495	496	Several bending/torsion vibrations	–
433	431	422	426	426	428	Several bending/torsion vibrations	–

Previous studies have elucidated the effects of different radiation sources on the FTIR spectra of PET, including UV radiation, gamma rays and ions irradiation, among others (Dworecki, Hasegawa, Sudlitz, & Wasik, 2000; Fechine et al., 2007; Nair, Sharma, Sharma, & Diwan, 2020; Prasad et al., 2011). These investigations have revealed discernible alterations in the molecular structure of the polymer, including changes in the intensities and positions of characteristic absorption peaks. For example, Fechine et al. (2007), reported that carboxyl acid end groups (–COOH) are formed during UV radiation due to a *photo--oxidation* process. This is evidenced by the increase of absorption at 3290 cm^{-1}, attributed to O–H stretching vibrations at carboxylic acid functional groups. Such groups are generated during the *photo-oxidation* of PET as a consequence of the reaction with the ester groups, leading to a significant reduction in mechanical properties. In a study by Nair et al. (2020), the effects of UVC irradiation were investigated at different exposure times. Their FTIR spectra indicated that the extent of damage to various bonds in the polymer is insignificant and increases with longer irradiation times. Damage induced by UVC irradiation is evident from the shifting of peaks (at 1235, 1093, 631 and 435 cm^{-1}) in the FTIR spectra to slightly higher wavenumbers. However, other bands in the PET FTIR spectra show resistance to UV irradiation and do not degrade further. Additionally, Prasad et al. (2011) investigated the effects of gamma irradiation at different doses on PET (up to 135 kGy), and it was found that no significant changes in the existing C–H and O–H stretching vibration of different types of H-bonds in the PET and also no alkyne group (at 3294 cm^{-1}) was detected in the region of 3600–2500 cm^{-1}. Moreover, their XRD and FTIR results support each other in finding no loss of crystallinity.

Thus, Dworecki et al. (2000) employed ion irradiation with N^{4+}, O^{5+} and Kr^{9+} ions, causing structural damage, attributed to several processes, including crosslinking of adjacent unsaturated radicals, amorphization of the crystalline fraction of the polymer, chain scission and oxidative reactions. These authors observed significant alterations in the infrared absorption bands within the spectral ranges of 3914–2970 cm^{-1}, 1683–1578 cm^{-1} and 631–506 cm^{-1}, which were primarily associated with the methylene group. Moreover, changes in the absorption spectra within the regions of 1740–1660 cm^{-1} and 1660–1600 cm^{-1} were ascribed to carbonyl group vibrations.

As appreciated in Fig. 2 (D-F), the normalized FTIR spectra of both non-irradiated PET samples and those irradiated with UVC for 1 h displayed minimal changes, with differences of less than 5% of transmittance respect to the mean value after UVC treatment. This observation confirms the resilience of bands within the PET FTIR spectra against UVC irradiation, demonstrating their resistance to further degradation. However, it is worth noting that a few subtle alterations were observed, as detailed below:

(i) A slight increase in the signal can be observed at 3290 cm^{-1}, attributed to O–H stretching vibrations in carboxylic acid end functional groups formed during PET *photo-oxidation* process.
(ii) UVC irradiation can induce the disruption of C–H stretching vibrations of both aromatic and aliphatic groups in the polymeric chain, leading to an increase in the FTIR signal at 2960 cm^{-1}.

(iii) The FTIR absorption peak at 1716 cm^{-1}, corresponding to C═O stretching vibrations in carboxylic acid end groups, is among the most intense peak in FTIR spectra. Significant alterations in peak intensity or position were assumed following UVC radiation treatment, based on existing literature. However, contrary to expectations, this peak does not exhibit any significant change in intensity or position.

(iv) UVC irradiation can induce a shift of peaks in the FTIR spectra to slightly higher wavenumbers, specifically from 1340 cm^{-1} to 420 cm^{-1}. This phenomenon becoming more pronounced as the thickness increases.

(v) Additionally, the peak centered at 1000 cm^{-1}, associated with the O–CH_2 bond aromatic moiety, exclusively arises in recycled materials. According to the literature, this observation could indicate the prevalence of degradation in recycled streams or the potential influence of isopropyl alcohol (IPA), which is commonly detected in bottles, as evidenced by the PET 1 sample (Fig. 2D) (Silva, 2016).

3.2. UVC-TL emissions of commercial dosimeters (TLD-100, TLD-200, TLD-400 and GR-200)

The investigation of PET shielding against UVC radiation holds significant importance in accurately detecting the potential radiation that reaches packaged food items. For such purpose, several commercial UVC detectors (Boronat et al., 2023), namely TLD-100 (LiF: Ti, Mg), TLD-200 (CaF_2: Dy), TLD-400 (CaF_2: Mn) and GR-200 (LiF: Mg, Cu, P), have been employed to check the yield of the UVC radiation concerning the thickness of the PET samples. This approach enables a qualitative discrimination between irradiated and non-irradiated PET packaging, thereby ensuring the quality and safety of food products.

Such commercial materials were employed as UVC radiation detectors for PET samples, and their corresponding UVC-induced TL emissions are presented in Fig. 3. Each of these emissions provides insights into fundamental characteristics associated with the interaction between UVC exposure and the distinct dosimeters, depending on the thickness of the PET material.

3.2.1. UVC effect on the TL response of TLD-100 (LiF: Ti, Mg)

As appreciated in Fig. 3 (A-C), the results reveal the presence of two groups of components in UVC-induced TL glow emissions:

(i) The TL glow emission in the lower temperature range (up to ~ 270 °C) consists of three maxima at ~ 165 °C, ~ 200 °C and ~ 250 °C, which are entirely linked to the ionizing component of the UVC radiation. The appearance of these maxima could be due to the formation of Ti^{4+} – OH^- defect complexes in conjunction with Mg^{2+} vacancies (referred to as Mg-dipoles), Mg^{2+} dipoles and/or Ti^{4+} – OH^-/Mg^{2+}-trimer defect complexes (Dryden & Shuter, 1973). Furthermore, several studies have demonstrated the significant presence of OH^- ions, with an ionic radius of 1.37 Å, replacing F^- ions (1.33 Å) within the LiF crystal lattice of the TLD-100 material. These hydroxyl groups are favorable to react with the metals found in the TLD-100 material, namely Ti^{4+} and Mg^{2+}. Consequently, it can be assumed that an increase in the concentration of OH^- ions within the matrix could enhance TL sensitivity (Weiss, Horowitz, & Oster, 2008).

Thus, PET 1 (Fig. 3A) and PET 2 (Fig. 3B) exhibit nearly identical

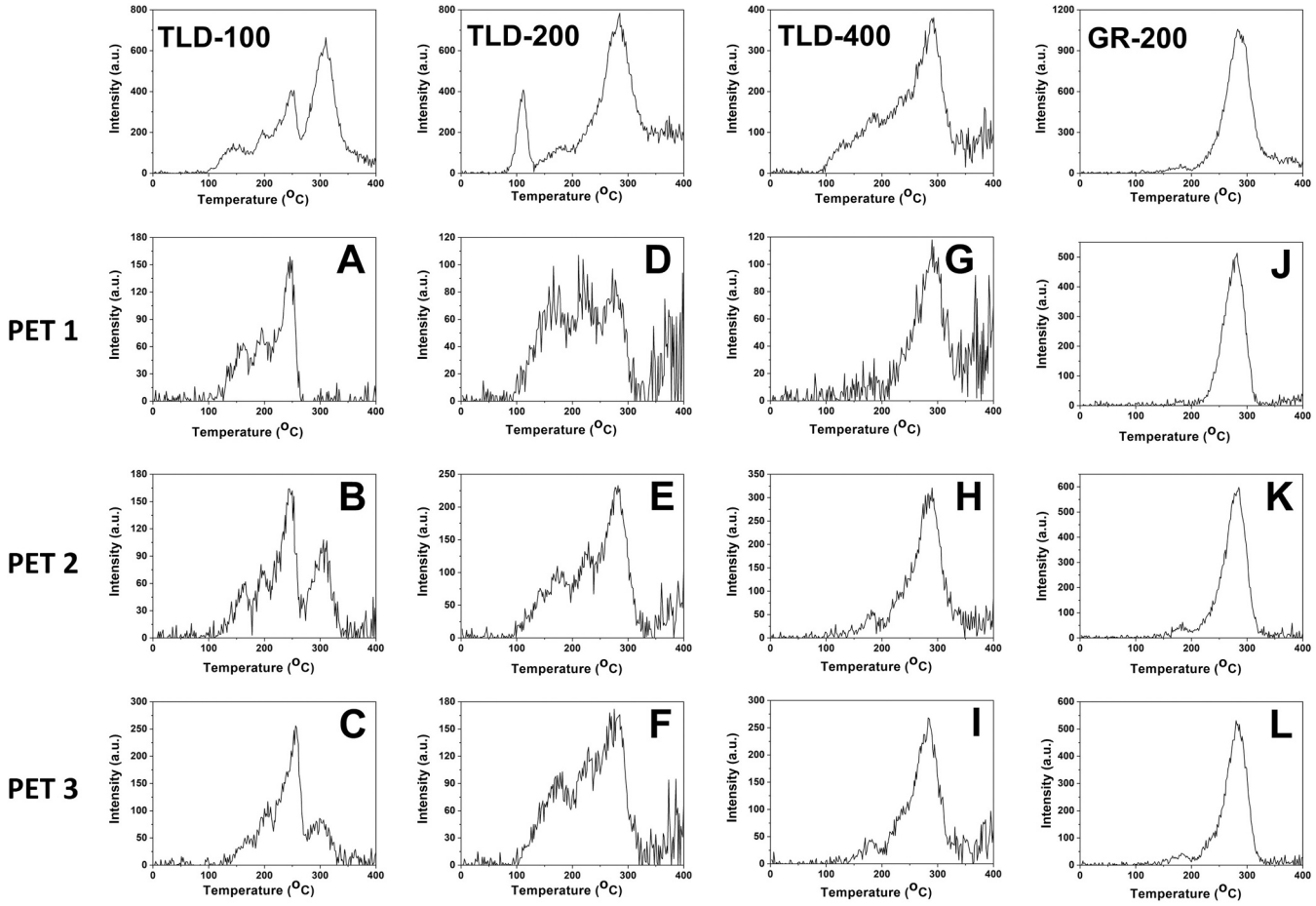

Fig. 3. UVC-induced TL spectra of PET food packaging samples with different thicknesses (PET 1, PET 2 and PET 3, corresponding respectively to the 2nd, 3rd and 4th line plots) and commercial dosimeters (TLD-100, TLD-200, TLD-400 and GR-200, corresponding respectively to the 1st, 2nd, 3rd and 4th columns). Note that the 1st line plot illustrates the UVC-induced TL spectra of the dosimeters without PET food packaging samples (Boronat et al., 2023).

peak intensity ratios of 2:2:5 and 2:3:6, respectively. In contrast, PET 3 (Fig. 3C) shows a comparable pattern with an intensity ratio of 1:2:5. These maxima consistently display apparently similar intensity ratios across different PET thicknesses. However, it is important to emphasize that even minor deviations should be taken into consideration. Specifically, while the peak centered at ~ 230 °C is less pronounced in PET 1 (Fig. 3A) and PET 2 (Fig. 3B), a change in slope is observed for PET 3 (Fig. 3C). This could suggest that as the thickness of the sample increases, it tends to absorb the non-ionizing component of UVC radiation while allowing the ionizing component to pass through. Therefore, variations in PET thicknesses used in this study (0.10, 0.42, and 0.60 mm), could result in significant differences in terms of the ionizing component of the UVC-induced TL glow emissions (up to ~ 270 °C).

And (ii), the TL emission at higher temperatures (over ~ 270 °C) is mainly associated with the non-ionizing component of the UVC radiation. In this case, a single TL emission peak is observed at ~ 305 °C and it serves as an indicator of the interaction between the non-ionizing component of UVC radiation and the dosimeters. PET 1 (Fig. 3A) exhibits a relatively low intensity value of ~ 15 a.u. within the emission peak centered at ~ 300 °C, while PET 2 (Fig. 3B) and PET 3 (Fig. 3C) display similar responses with intensity values of ~ 90 and ~ 70 a.u., respectively. This consistent response to the non-ionizing component suggests a similar sensitivity to UVC radiation in the TLD-100 under these increased PET thicknesses (0.42, and 0.60 mm), which could be related to the permeability of the PET samples to the non-ionizing component of UVC radiation.

In summary, the TLD-100 dosimeter exhibits a high temperature signal peaked at ~ 305 °C, which is associated with the non-ionizing component of UVC radiation and is predominantly in PET samples of greater thickness (PET 2 and PET 3), displaying similar pattern observed in the TLD-100 dosimeter without plastic sample (1:1:3:4) in terms of both curve shape and intensity relationships. However, this signal is not consistently observable across all PET samples, in this case, limitations become pronounced when thinner plastic samples are considered (PET 1). This significant dispersion of the results indicates that TLD-100 does not appear to be a potential UVC detector under these measurement conditions. Furthermore, FTIR analysis does not reveal any discernible degradation of the PET materials following UVC exposure, confirming their robustness under these experimental conditions.

3.2.2. UVC effect on the TL response of TLD-200 (CaF_2: Dy)

The UVC-induced TL emissions from the TLD-200 dosimeter employed under the PET samples (Fig. 3 (D-F)) show the existence of three distinct groups of components:

(i) And (ii), the TL glow emission occurring within the temperature range from ~ 165 °C to ~ 230 °C, would be associated with non-ionizing component of the UVC irradiation.

Conversely, (iii) the TL emission at higher temperatures, centered at ~ 280 °C and extending up to ~ 350 °C, would be mostly linked to the ionizing component of the UVC radiation. According to Boronat et al. (2023), these maxima could be attributed to structural defects and impurities induced by Dy^{3+} ions, with an atomic radii of 1.59 Å, residing within Ca^{2+} sites (1.74 Å) in the CaF_2 crystal lattice.

Considering the relative intensity values of these three groups of components, PET 1 (Fig. 3D) displays a ratio of 1:1:1, PET 2 (Fig. 3E) exhibits a ratio of 3:4:7 and PET 2 (Fig. 3F) shows a ratio of 3:4:5. It is important to note that the thickness of the samples (0.10, 0.42, and 0.60 mm) used in this study result in significant variations within the temperature range of ~ 165 °C to 230 °C, attributed to the non-ionizing component of the UVC irradiation. Moreover, one can also appreciate differences concerning the ionizing component of the UVC-induced TL glow emissions (peaked at ~ 280 °C). This phenomenon could be linked to the ability of the PET samples to allow the transmission of the non-ionizing component of the UVC radiation. Significantly, for the thicker PET samples (PET 2 with 0.42 mm and PET 3 with 0.60 mm), the increase in both TL signals is more prominent, especially for PET 2.

Therefore, the TLD-200 dosimeter demonstrates effective UVC detection capabilities by consistently displaying UVC response levels within the temperature range from ~ 165 °C to 230 °C (linked to the non-ionizing component of the UVC radiation) for the three PET samples studied. Samples exhibit distinct behavior compared to the TLD-200 dosimeter without a plastic sample (4:1:8) in both curve shape and intensity relationships. As previously discussed, these observations primarily concern PET samples with greater thickness. When thinner plastic samples are examined, limitations become more evident, requiring careful interpretation. Moreover, FTIR analysis indicates that there is no observable degradation of the PET materials after exposure to UVC, providing additional evidence of the durability of these materials in the experimental settings.

3.2.3. UVC effect on the TL response of TLD-400 (CaF_2: Mn)

As depicted in Fig. 3 (G-H), UVC-induced TL emissions on TLD-400 under PET samples exhibit behavior consistent with previous characterizations of this specific material under UVC radiation (Boronat et al., 2023). These emissions can be classified into two distinct groups of components:

(i) Several TL glow emissions displaying up to ~ 200 °C, attributed to the influence of the non-ionizing component of the UVC radiation. These emissions could be related to structural defects and the presence of Mn^{2+} impurities (with atomic radii of 1.17 Å) that are placed in Ca^{2+} sites (1.74 Å) in the CaF_2 crystal lattice (Topaksu, Correcher, & Garcia-Guinea, 2016; Yazici, Bedir, & Sökücü, 2007).

And (ii), a broad maximum centered at ~ 280 °C, mainly associated with the ionizing component of UVC radiation.

Thus, the TL signal exhibited by TLD-400 under PET 1 sample (Fig. 3G) is almost negligible at lower temperatures, suggesting minimal response to UVC radiation up to ~ 200 °C, and this could be due to the minimum thickness of the sample (0.10 mm). Conversely, it displays a broad peak centered at ~ 280 °C, with an intensity of ~ 90 a.u., which can be attributed to the ionizing component of the UVC radiation. However, TLD-400 under PET 1 displays the lowest intensity value up to ~ 200 °C (linked to UVC radiation), when compared to signals obtained from TLD-400 materials placed under PET 2 and PET 3 samples. Due to such limited radiation transmission by the PET 1 sample, it is expected that UVC radiation will have a reduced impact on the packaged food during the irradiation process.

On the contrary, TL signal from TLD-400 under both PET 2 (Fig. 3H) and PET 3 (Fig. 3I) exhibits a 1:7 ratio of relative intensity values for the prominent components centered at ~ 175 °C and 280 °C, due to the ionizing component of UVC radiation. This suggests that the thicker PET samples have a negligible impact on their response to UVC radiation (at ~ 175 °C), and both samples have a similar ability to allow the passage of the UVC light. Moreover, the TLD-400 dosimeter without plastic sample displays 1:4 ratio of relative intensity values for these groups of components.

Therefore, the TLD-400 dosimeter displays a TL signal observed up to ~ 200 °C, linked to the UVC radiation and is mainly relevant for thicker PET samples (PET 2 and PET 3). However, the signal is not uniformly detectable in all PET samples, and its limitations become more apparent, especially when evaluating thinner plastic samples (PET 1). The substantial variability in results suggests that TLD-400 could not be a suitable dosimeter for UVC detection under these measurement conditions. Additionally, FTIR analysis confirms the absence of any detectable degradation in PET materials following UVC exposure, further supporting the durability of these materials in the experimental conditions.

3.2.4. UVC effect on the TL response of GR-200 (LiF: Mg, Cu, P)

UVC-induced TL emissions of PET samples on a GR-200 material (Fig. 3 (J-L)) display a peak centered at ~ 280 °C, attributed to the ionizing component of the UVC radiation. This emission could be associated with the recombination of crystalline defects such us, H-F defects (color centers in the LiF crystal lattice) and V_k −e centers (related to

vacancies and electron traps) (Yang, Wang, Townsend, & Gao, 2008). This sensitivity to the ionizing component of the UVC radiation is observed at higher temperatures (at ~ 280 °C), with a negligible TL signal at lower temperatures (at ~ 180 °C). Consequently, GR-200 could serve as a suitable dosimeter for detecting ionizing radiation, whereas it is unable to discriminate between UVC and ionizing radiation (Boronat et al., 2023).

Hence, PET 1 (Fig. 3J) displays an intensity of ~ 460 a.u. in the peak centered at ~ 280 °C, with an insignificant TL signal at lower temperatures. In contrast, both PET 2 (Fig. 3K) and PET 3 (Fig. 3L) exhibit a similar pattern, showing an intensity ratio of 1:14 between the two main signals centered at ~ 180 °C and ~ 280 °C (associated with the ionizing component of UVC radiation). As previously outlined, these findings are primarily applicable to thicker PET samples. Analyzing thinner plastic samples presents challenges, requiring careful and thorough interpretation. Additionally, FTIR analysis further corroborates the durability of PET materials under the experimental conditions, as it reveals no discernible degradation following exposure to UVC radiation.

4. Conclusions

The present study enhances our understanding of the intricate relationship between UVC radiation and PET materials, particularly in post-packaging irradiation treatment for food safety and quality control. UVC radiation can penetrate PET samples regardless of their thickness; however, its efficiency is significantly influenced by the thickness of the material. This phenomenon underscores the crucial importance for food packaging companies to comprehensively evaluate the chemical composition and thickness of their materials for optimal UVC post-packaging treatment.

These preliminary results demonstrate the capacity of UVC radiation to cause intricate chemical alterations in the molecular structure of PET, as evidenced by the subtle alterations observed in FTIR spectra. Specifically, UVC could induce: (i) the formation of carboxylic acid end groups due to increased O−H stretching vibrations (at 3290 cm^{-1}), (ii) disruptions in both aromatic and aliphatic C−H stretching vibrations (at 2960 cm^{-1}) and (iii) a shift in FTIR peaks to slightly higher wavenumbers, which becomes more pronounced with increasing thickness. Furthermore, the stability of the C═O stretching peak (at 1716 cm^{-1}) indicates resistance of PET samples to degradation under UVC radiation.

On the other hand, an in-depth analysis of TL emissions provides detailed insights into the capabilities and limitations of several dosimeter materials in UVC radiation detection. The TLD-200 dosimeter demonstrates potential as a UVC detector due to its UVC-TL response ranging from ~ 165 °C to ~230 °C, linked to the non-ionizing component of the UVC radiation. In contrast, TLD-100, TLD-400 and GR-200 dosimeters do not exhibit promise as UVC detectors due to the significant dispersion in results, which are not consistently observed across all PET samples. These discrepancies are particularly noticeable in thicker PET samples, underscoring the importance of sample thickness in accurate detection and interpretation of results.

Thus, this methodology confirms the capability to reliably detect food product irradiation after just one hour of exposure, enhancing confidence in detection even during prolonged UVC exposure. Consequently, this comprehensive analysis has expanded our scientific understanding and offers practical insights for industries using UVC-PET irradiated products.

CRediT authorship contribution statement

C. Boronat: Investigation, Writing - Original Draft and Writing - Review & Editing. **V. Correcher:** Investigation, Writing - Review & Editing and Supervision. **J. C. Bravo-Yagüe:** Investigation, Writing - Review & Editing and Supervision.

Declaration of Competing Interest

The authors declare that they have no known competing financial interests or personal relationships that could have appeared to influence the work reported in this paper.

Data availability

Data will be made available on request.

Acknowledgments

Cecilia Boronat thanks for the predoctoral researcher contract with UNED-SANTANDER associated under the UNESCO Chair, for the support extended under the program "*UNESCO Chair on Science and Innovation for Sustainable Development: Global Food Production and Safety*".

References

Andrady, A. L., Heikkilä, A. M., Pandey, K. K., Bruckman, L. S., White, C. C., Zhu, M., & Zhu, L. (2023). Effects of UV radiation on natural and synthetic materials. *Photochemical & Photobiological Sciences, 22*, 1177–1202. https://doi.org/10.1007/s43630-023-00377-6

Belović, M., Kevrešan, Ž., Pestorić, M., & Mastilović, J. (2015). The influence of hot air treatment and UV irradiation on the quality of two tomato varieties after storage. *Food Packaging and Shelf Life, 5*, 63–67. https://doi.org/10.1016/j.fpsl.2015.06.002

Ben-Fadhel, Y., Cingolani, M. C., Li, L., Chazot, G., Salmieri, S., Horak, C., & Lacroix, M. (2021). Effect of γ-irradiation and the use of combined treatments with edible bioactive coating on carrot preservation (Article) *Food Packaging and Shelf Life, 28*, Article 100635. https://doi.org/10.1016/j.fpsl.2021.100635.

Boronat, C., Correcher, V., Bravo-Yagüe, J. C., Sarasola-Martin, I., Garcia-Guinea, J., & Benavente, J. F. (2023). Comparing the effect of electron beam, beta and ultraviolet C exposure on the luminescence emission of commercial dosimeters (Article) *Spectrochimica Acta Part A: Molecular and Biomolecular Spectroscopy, 295*, Article 122571. https://doi.org/10.1016/J.SAA.2023.122571.

Bøtter-Jensen, L., & Duller, G. A. T. (1992). A new system for measuring optically stimulated luminescence from quartz samples. *International Journal of Radiation Applications and Instrumentation Part D Nuclear Tracks and Radiation Measurements, 20*(*4*), 549–553. https://doi.org/10.1016/1359-0189(92)90003-E

Chen, Z., Hay, J. N., & Jenkins, M. J. (2012). FTIR spectroscopic analysis of poly (ethylene terephthalate) on crystallization. *European Polymer Journal, 48*(*9*), 1586–1610. https://doi.org/10.1016/j.eurpolymj.2012.06.006

Chun, H. H., Kim, J. Y., Lee, B. D., Yu, D. J., & Song, K. B. (2010). Effect of UV-C irradiation on the inactivation of inoculated pathogens and quality of chicken breasts during storage. *Food Control, 21*(*3*), 276–280. https://doi.org/10.1016/j.foodcont.2009.06.006

Correcher, V., & Delgado, A. (1998). On the use of natural quartz as transfer dosemeter in retrospective dosimetry. *Radiation Measurements, 29*(*3–4*), 411–414. https://doi.org/10.1016/S1350-4487(98)00040-7

Correcher, V., & Garcia-Guinea, J. (2011). Application of the EN 1788 European standard for the control of saffron, pepper and blends. *Food Control, 22*(*2*), 173–179. https://doi.org/10.1016/j.foodcont.2010.05.020

Correcher, V., & Garcia-Guinea, J. (2013). Potential use of the activation energy value calculated from the thermoluminescence glow curves to detect irradiated food. *Journal of Radioanalytical and Nuclear Chemistry, 298*(*2*), 821–825. https://doi.org/10.1007/s10967-013-2473-3

Day, M., & Wiles, D. M. (1972). Photochemical degradation of poly(ethylene terephthalate). III. Determination of decomposition products and reaction mechanism. *Journal of Applied Polymer Science, 16*, 203–215. https://doi.org/10.1002/app.1972.070160118

Delgado, A., Unamuno, V., Muñiz, J. L., Correcher, V., & Gómez Ros, J. M. (1996). A simple UV irradiator for low dose reassessment with LiF TLD-100. *Radiation Protection Dosimetry, 67*(*4*), 303–306. https://doi.org/10.1093/oxfordjournals.rpd.a031834

Donelli, I., Freddi, G., Nierstrasz, V. A., & Taddei, P. (2010). Surface structure and properties of poly-(ethylene terephthalate) hydrolyzed by alkali and cutinase. *Polymer Degradation and Stability, 95*(*9*), 1542–1550. https://doi.org/10.1016/j.polymdegradstab.2010.06.011

Dryden, J. S., & Shuter, B. (1973). The dependence of the thermoluminescence of LiF: Mg^{2+} crystals on the state of aggregation of the Mg^{2+} ions. *Journal of Physics D: Applied Physics, 6*, 123–130. https://doi.org/10.1088/0022-3727/6/1/316

Dworecki, K., Hasegawa, T., Sudlitz, K., & Wasik, S. (2000). Modification of electrical properties of polymer membranes by ion implantation. *Nuclear Instruments and Methods in Physics Research, Section B: Beam Interactions with Materials and Atoms, 166–167*, 646–649. https://doi.org/10.1016/S0168-583X(99)01218-5

EN 1788. (2001). Thermoluminescence detection of irradiated food from which silicate minerals can be isolated. Retrieved from EN 1788 - English version Foodstuffs-Thermoluminescence detection of irradiated food from which silicate minerals can be i. (europa.eu). Accessed September 10, 2001. Belgium, European Committee for Standardization.

Fechine, G. J. M., Souto-Maior, R. M., & Rabello, M. S. (2007). Photodegradation of multilayer films based on PET copolymers. *Journal of Applied Polymer Science, 104* (*1*), 51–57. https://doi.org/10.1002/app.24517

Fernández-Menéndez, T., García-López, D., Argüelles, A., Fernández, A., & Viña, J. (2020). Industrially produced PET nanocomposites with enhaced properties for food packaging applications (Article) *Polymer Testing, 90*, Article 106729. https://doi.org/10.1016/j.polymertesting.2020.106729.

Foschi, C., Giorgi, B., Ambretti, S., Lazzarotto, T., & Violante, F. S. (2023). Real-life assessment of the ability of an ultraviolet C lamp (SanificaAria 200, Beghelli) to inactivate airborne microorganisms in a healthcare environment (Article) *Life, 13*(*5*), 1221. https://doi.org/10.3390/life13051221.

Ghazala, S. (2020). Part 179—Irradiation in the production, processing and handling of food. *The CRC master keyword guide for food* (pp. 1054–1059). CRC Press. https://doi.org/10.1201/9780203504529-58

Giaganini, G., Cifelli, M., Biagini, D., Ghimenti, S., Corti, A., Castelvetro, V., Domenici, V., & Lomonaco, T. (2023). Multi-analytical approach to characterize the degradation of different types of microplastics: Identification and quantification of released organic compounds. *Molecules, 28*(*3*), 1382. https://doi.org/10.3390/molecules28031382

Guerrero-Beltrán, J. A., & Barbosa-Cánovas, G. V. (2004). Review: Advantages and limitations on processing foods by UV light. *Food Science and Technology International, 10*(*3*), 137–147. https://doi.org/10.1177/1082013204044359

Hu, K., Huyan, Z., Ding, S., Dong, Y., & Yu, X. (2020). Investigation on food packaging polymers: Effects on vegetable oil oxidation (Article) *Food Chemistry, 315*, Article 126299. https://doi.org/10.1016/j.foodchem.2020.126299.

Jamalzadeh, M., & Sobkowicz, M. J. (2022). Review of the effects of irradiation treatments on poly(ethylene terephthalate) (Article) *Polymer Degradation and Stability, 206*, Article 110191. https://doi.org/10.1016/j.polymdegradstab.2022.110191.

Junqueira-Gonçalves, M. P., Alarcón, E., & Niranjan, K. (2013). Development of antifungal packaging for berries extruded from recycled PET. *Food Control, 33*(*2*), 455–460. https://doi.org/10.1016/j.foodcont.2013.03.031

McKeever, S. W. S. (1986). Mechanisms of thermoluminescence production in materials for radiation dosimetry. *Radiation Protection Dosimetry, 17*, 431–435. https://doi.org/10.1093/oxfordjournals.rpd.a079854

Mikac, L., Csáki, A., Zentai, B., Rigó, I., Veres, M., Tolić, A., Gotić, M., & Ivanda, M. (2023). UV irradiation of PET and PP and detection of formed microplastic particles down to 1 μm. *ChemPlusChem*, Article e202300497. ⟨https://api.semanticscholar.org/CorpusID:264488250⟩.

Nair, A., Sharma, P., Sharma, V., & Diwan, P. K. (2020). Effect of UV-irradiation on the optical properties of transparent PET polymeric foils. *Materials Today: Proceedings, 21* (Part 4), 2105–2111. https://doi.org/10.1016/j.matpr.2020.01.330

Paiva, R., Wrona, M., Nerín, C., & Cruz, S. A. (2022). Hydrogenated amorphous carbon film deposited by plasma on recycled polypropylene as a functional barrier to hazardous migrants (Article) *Food Packaging and Shelf Life, 33*, Article 100864. https://doi.org/10.1016/j.fpsl.2022.100864.

Prajapati, U., Asrey, R., Varghese, E., Singh, A. K., & Pal Singh, M. (2021). Effects of postharvest ultraviolet-C treatment on shelf-life and quality of bitter gourd fruit during storage (Article) *Food Packaging and Shelf Life, 28*, Article 100665. https://doi.org/10.1016/j.fpsl.2021.100665.

Prasad, S. G., De, A., & De, U. (2011). Structural and optical investigations of radiation damage in transparent PET polymer films (Article) *International Journal of Spectroscopy, 2011*, Article 810936. https://doi.org/10.1155/2011/810936.

Silva, E.A. (2016). Raman Spectroscopy and Chemometrics Applied to Recycled Polyethylene Terephthalate. ⟨http://www.lib.ncsu.edu/resolver/1840.16/11376⟩. Accessed June 28, 2016. North Carolina State University.

Soro, A. B., Noore, S., Hannon, S., Whyte, P., Bolton, D. J., O'Donnell, C., & Tiwari, B. K. (2021). Current sustainable solutions for extending the shelf life of meat and marine products in the packaging process (Article) *Food Packaging and Shelf Life, 29*, Article 100722. https://doi.org/10.1016/j.fpsl.2021.100722.

Tao, T., Ding, C., Han, N., Cui, Y., Liu, X., & Zhang, C. (2019). Evaluation of pulsed light for inactivation of foodborne pathogens on fresh-cut lettuce: Effects on quality attributes during storage (Article) *Food Packaging and Shelf Life, 21*, Article 100358. https://doi.org/10.1016/j.fpsl.2019.100358.

Topaksu, M., Correcher, V., & Garcia-Guinea, J. (2016). Luminescence emission of natural fluorite and synthetic CaF_2: Mn (TLD-400). *Radiation Physics and Chemistry, 119*, 151–156. https://doi.org/10.1016/j.radphyschem.2015.10.002

Weiss, D., Horowitz, Y. S., & Oster, L. (2008). Delocalized recombination kinetic modeling of the LiF: Mg, Ti (TLD-100) glow peak 5 TL system. *Radiation Measurements, 43*(*2*−*6*), 254–258. https://doi.org/10.1016/j.radmeas.2007.10.026

Yang, B., Wang, L., Townsend, P. D., & Gao, H. (2008). Comparison between the low temperature thermoluminescence spectra in annealed LiF: Mg, Cu, LiF: Mg, Cu, P and LiF: Mg, Cu, Si. *Nuclear Instruments and Methods in Physics Research, Section B: Beam Interactions with Materials and Atoms, 266*(*11*), 2581–2586. https://doi.org/10.1016/j.nimb.2008.03.199

Yazici, A. N., Bedir, M., & Sökücü, A. S. (2007). The analysis of dosimetric thermoluminescent glow peak of CaF_2:Mn after β-irradiation. *Nuclear Instruments and Methods in Physics Research, Section B: Beam Interactions with Materials and Atoms, 259* (2), 955–965. https://doi.org/10.1016/j.nimb.2007.02.104

Zhang, L. Y., Song, W. M., Li, P., Wang, J. S., Liu, Y., & Zhu, P. (2022). Green flame-retardant coatings based on iron alginate for polyester fabrics: Thermal stability, flame retardancy and mechanical properties (Article) *Polymer Degradation and Stability, 206*, Article 110207. https://doi.org/10.1016/j.polymdegradstab.2022.110207.